Paleogene V-shaped basins and Neogene subsidence of the Northern Lesser Antilles Forearc

Boucard M.[1-2], Marcaillou B.[2], Lebrun J.-F.[1], Laurencin M.[3], Klingelhoefer, F.[4], Laigle, M.[2], Lallemand, S.[5], Schenini L.[2], Graindorge D.[3], Cornée J.-J[1-5], Münch, P.[5], Philippon M.[1], and the ANTITHESIS 1, 3 and GARANTI Scientific Teams.

1 Géosciences Montpellier, Université des Antilles, Université de Montpellier, CNRS, Campus de Fouillole, Pointe-à-Pitre, Guadeloupe (FWI), France

2 GéoAzur, Université Côte d'Azur, CNRS, Observatoire de la Côte d'Azur, IRD, 250 Avenue Albert Einstein, 06560 Valbonne, France

3 Laboratoire Géosciences Océan, CNRS-UBO-UBS, Université Bretagne Pays de Loire (UBL), Brest, Institut Universitaire Européen de la Mer, rue Dumont Durville, F-29280, Plouzané, France.

4 Géosciences Marines, Ifremer, ZI de la Pointe de Diable, CS 10070, 29280 Plouzané France

5 Géosciences Montpellier, Université de Montpellier, CNRS, Université des Antilles, Place Eugène Bataillon, 34095 Montpellier, France

The ANTITHESIS and GARANTI cruise teams include: Agranier, A.[3], Arcay, D.[5], Audemard, F.[6], Beslier, M.-O.[2], Boucard, M.[1], Bouquerel, H.[7], Conin, M.[8], Cornée, J.J. [5], Crozon, J.[4], Dellong, D.[4], De Min, L.[1], de Voogd, B.[9], Evain, M.[4], Fabre, M.[1], Gay, A.[5], Graindorge, D.[3], Gwandai, W.[2], Heuret, A.[10], Klingelhoefer, F.[4], Laigle, M.[2], Lallemand, S.[5], Laurencin, M.[3], Lebrun, J.-F.[1], Legendre, L.[1], Léticée, J.L.[1], Lucazeau, F.[7], Mahamat, H.[2], Malengros, D.[2], Marcaillou, B.[2], Mazabraud, Y.[1], Mercier de Lepinay, B.[2], Olliot, E.[5], Oregioni, D.[2], Padron, C.[4], Pichot, T.[4], Prunier, C.[3], Quillévéré, F.[11], Ratzov, G.[2], Renouard, A.[2], Rolandonne, F.[12], Rousset, D. [9], Schenini, L.[2], Thomas, Y.[4], Vitard, C.[2], Yates, B.[2]

6 Departamento de Ciencias de la Tierra, Fundacion Venezolana de Investigaciones Sismologicas (Funvisis), Caracas 1070, Venezuela.

7 Université de Paris, Institut de physique du globe de Paris, CNRS, Paris, France

8 Université de Lorraine, CNRS, CREGU, GeoResources Lab, Nancy School of Mines, Campus ARTEM, Nancy, France

9 Université de Pau et des Pays de l'Adour, CNRS UMR 5212, Pau, France.

10 Géosciences Montpellier, Université de la Guyane, Université de Montpellier, CNRS, Campus de Cayenne, Guyane, France.

11 Laboratoire de Géologie de Lyon: Terre, Planètes, Environnement, UMR CNRS 5276, Université Lyon 1, France

12 Sorbonne Universités, UPMC Université Paris 06, CNRS, Institut des Sciences de la Terre de Paris (ISTeP), F75005 Paris, France

Abstract

Oblique collision of buoyant provinces against subduction zones frequently results in individualizing and rotating regional-scale blocks. In contrast, the collision of the Bahamas Bank against the Northeastern Caribbean Plate increased the margin convexity triggering forearc fragmentation into small-scale blocks. This deformation results in a prominent >450-km-long sequence of V-shaped basins that widens trenchward separated by elevated spurs, in the Northern Lesser Antilles (NLA, i.e. Guadeloupe to Virgin Island). In absence of deep structure imaging, various competing models were proposed to account for this faults-bounded Basins-and-Spurs System. High-resolution bathymetric and deep multichannel seismic data acquired during cruises ANTITHESIS1-3, reveal a drastically different tectonic evolution of the NLA forearc.

During Eocene-Oligocene time, the NLA margin accommodated the Bahamas Bank collision and the consecutive margin convex bending by trench-parallel extension along N40-90°-trending normal faults, opening V-shaped valleys in the forearc. Backarc spreading in the Kalinago Basin and block rotations went along with this tectonic phase, which ends up with tectonic uplifts and an earliest-middle Miocene regional emersion phase. Post middle Miocene, regional subsidence and tectonic extension in the forearc is partly accommodated along the newly-imaged N300°-trending, 200-km-long Tintamarre Normal Faults Zone. This drastic subsidence phase reveals vigorous margin basal erosion, which likely generated the synchronous westward migration of the volcanic arc. Thus, unlike widely-accepted previous theoretical models, the first deep seismic images in the NLA forearc show that the NE-SW faulting and the prominent V-Shaped valleys result from a past and sealed tectonic phase related to the margin bending and consecutive blocks rotation.

1 Introduction

Worldwide, forearc trench-perpendicular basins are interpreted as the result of trench-parallel extension possibly due to either strain partitioning as at the Aleutians (Ryan and Scholl, 1989) and Ryukyu (Nakamura, 2004) subduction zones, and/or to increasing margin curvature as at the Marianas (Heeszel et al., 2008) and Hellenic trenches (Angelier, 1978; Mascle and Martin, 1990). In more extreme cases, widespread deformation of forearc domains result from the collision of buoyant crustal features (e.g. oceanic plateaus, seamount chains or continental fragments) which is prone to generate bending and rotation of subduction zones (e.g. Vogt et al., 1976). Strongly curved convergent plate boundaries are subject to along-strike variations in subduction obliquity and thus commonly associated with large-scale rigid body rotation of forearc microplates (McCabe, 1984). A compilation of plate convergent boundaries supports this relationship between lateral change from subduction to collision, plate boundary bending and forearc rotation (Wallace et al., 2009). These authors suggested that the indentor apply a torque force on the upper plate due to continuous subduction away from the indentor depending on the ability of the slab to roll back. Thus, most of the time, the collision triggers rotation of large-scale forearc blocks, sometimes large enough to be named “microplate”. In this context, various parameters control the trench motion velocity, the slab roll-back or anchoring and the plate drag resulting in varying convexity for the subduction zones worldwide. These parameters include mantle rheology and toroidal flow at slab edges, slab-mantle rheology contrast, along-strike variations in slab age and density, along-strike variations in interplate friction (Schellart, 2010). Margin bending and block rotations define an upper plate deformation pattern, possibly including backarc basin spreading (Boutelier and Cruden, 2013; Wallace et al., 2009) trench-parallel strike-slip fault and forearc stretching that depend on the amount of trench bending (Heeszel et al., 2008).

At the Northern Lesser Antilles (NLA) margin, a prominent regional sequence of transverse V-shaped valleys opening trenchward, separated by 4-6-km high spurs, dissects the inner slope of the forearc from La Désirade Island to Anguilla Island (Figure 1 and Figure 2). No consensus has been reached about the age and the causes for this tectonic pattern. Previous studies suggested that northward increasing strain partitioning, due to the curved shape of the subduction zone, caused along-strike stretching within a northwestward-moving forearc sliver (Lopez et al., 2006) bounded westward by a left-lateral strike-slip fault along the volcanic active arc (Feuillet et al., 2011; Feuillet et al., 2002). According to this model, forearc stretching triggers the currently active N40-90°-trending normal faults, which control vertical relative motion at the V-shaped basins flanks. This model implies long-term strong mechanical coupling along the interplate contact of a curved margin, which is somewhat controversial with

the lack of crustal-scale transcurrent tectonic systems south of the Anegada Passage (Laurencin et al., 2019). Other studies suggest that, since the late Paleocene–early Eocene time, the collision and westward drifting of the Bahamas Bank with the Northeastern Caribbean Plate has likely caused the current margin convexity (Pindell and Barrett, 1990) (Figure 1), the margin segmentation in regional-scale crustal blocks (e.g. Pindell and Kennan, 2009) and blocks rotations (e.g. Mann et al., 2005).

In this study, we raise the question of the relationship between the widespread, pervasive and deep-rooting fracturing of the NLA forearc Basins-and-Spurs System and the convex margin bending. Absence of detailed bathymetric data and deep seismic images across the Basins-and-Spurs System previously precluded detailed investigations of the NLA forearc deformation chronology. As a result, chronology and causal relationships between continental collision, margin bending, increasing convergence obliquity and forearc fragmentation in transverse (perpendicular to the trench) basins need to be evaluated.

During SISMANTILLES 1 (Hirn, 2001), SISMANTILLES 2 (Laigle et al., 2007), ANTITHESIS 1 (Marcaillou and Klingelhoefer, 2013a, b) and ANTITHESIS 3 (Marcaillou and Klingelhoefer, 2016) cruises onboard French R/Vs *Nadir*, *L'Atalante* and *Pourquoi Pas?*, we recorded high resolution bathymetric, low frequency Multi-Channel Seismic (MCS) and Wide-Angle Seismic (WAS) data in order to decipher the tectonic deformation at the NLA Margin. In this study, we focus onto the margin tectonic evolution that resulted in the Basins-and-Spurs System, which dissects the NLA Forearc. We describe the sedimentary architecture and tectonic deformation of the northernmost features of this system. The newly-imaged Saint-Barthelemy Valley and bordering Tintamarre and Barbuda Spurs (Figure 3) highlight the tectono-stratigraphic evolution of the area. Correlating our seismic interpretation to onshore geological constraints and upper-margin basins stratigraphy (Cornée et al., 2020; De Min et al., 2015; Legendre et al., 2018) allows us to propose a chronostratigraphic interpretation of the tectonic evolution of the studied area. As a result, this study revises fundamentally the formation and tectonic evolution of the V-shaped Basins-and-Spurs System in the frame of a bending convergent margin.

2 Geological Settings

The Lesser Antilles Subduction zone is located at the eastern edge of the Caribbean Plate where the North and South American Plates subduct westward at ~20 Km/Myr in a ~N254° direction beneath the Lesser Antilles Margin (DeMets et al., 2000) (Figure 1). The margin convex shape generates a northward increase in plate convergence obliquity, from ~0° offshore of Guadeloupe to more than 70° offshore of Puerto-Rico. Since the early Eocene,

plates relative motion has remained mostly constant and absolute motion of the Caribbean Plate is nearly stationary in a mantle reference frame (Boschman et al., 2014). Thus, the North American Plate has moved westward, leading the Bahamas Bank to sweep along the northern Caribbean Plate Margin. Since the late Paleocene–early Eocene time, the collision of the bank with the Greater Caribbean Arc has resulted in a major plate boundary re-organization (e.g. Escalona and Mann, 2011; Pindell and Kennan, 2009). The plate boundary relocated along the left lateral Cayman Through that propagated from west to east, to transpressive fault zones across Hispaniola (Leroy et al., 2000; Mann et al., 1995).

The NLA Subduction Zone has generated three distinct volcanic arcs: 1/ the late Cretaceous – Paleocene arc at the Aves Ridge (Bouysse et al., 1985; Neill et al., 2011), 2/ the remnant middle Eocene – earliest Miocene Lesser Antilles Arc in the current forearc to the north of Martinique Island (Bouysse and Westercamp, 1990; Legendre et al., 2018; Martin-Kaye, 1969) and 3/ the early Pliocene - present day Lesser Antilles active Arc, located to the west of the previous arc (Lindsay et al., 2005) (Figure 1). The NLA forearc basins developed, at least partly, during the post early Miocene landward migration of the volcanic Lesser Antilles Arc recording the tectonic evolution for this time period. Bouysse and Westercamp (1990) suggested that this arc migration resulted from a slab shallowing subsequent to a slab rupture after the Bahamas Bank collision. Alternatively, Allen et al. (2019) proposed that the slab has shallowed underneath the Lesser Antilles in response to constraints imposed by the neighboring American Plates.

The reduced size of the ~30-km-wide accretionary wedge (Figure 2), that fronts the NLA forearc, contrasts with the >100-km-wide prism offshore of Guadeloupe and farther south (Deville and Mascle, 2012; Westbrook et al., 1984). This accretionary prism thus narrows northward as the South American continental sources of sediments recedes (Deville et al., 2015). The outer forearc domain corresponds with an interpreted transition zone made of imbricated and underplated material or damage upper plate igneous basement covered with deep forearc sedimentary basins (Bangs et al., 2003; Evain et al., 2013; Laigle et al., 2013) (Figure 2). To the northwest of Barbuda Island, the trench-parallel left-lateral strike-slip Bunce Fault separates the accretionary wedge from the outer forearc (Laurencin et al., 2019), (Figure 1 and Figure 2). This fault accommodated the left-lateral component of the plate convergence, revealing active strain partitioning along the oblique plate boundary to the northwest of Barbuda (Laurencin et al., 2019; ten Brink and Lin, 2004). Farther west, at the Puerto Rico and the Virgin Islands (PRVI) Margin, the Bunce and Bowin left-lateral strike-slip faults connect to the northern Hispaniola lithospheric transpressive faults, which bound the Bahamas Bank – Hispaniola collisional system (Mann et al., 2005; Rodríguez-Zurrunero et al., 2019; ten Brink and Lin, 2004).

The boundary between the inner and the outer forearc is located at the margin slope break at the easternmost extent of the Basins-and-Spurs System (Figure 2). Up slope, the inner forearc alternates remnant volcanic arc islands (Antigua, St Barthelemy, St Martin) and Neogene to Pleistocene carbonate platform, some of which being emerged (Marie-Galante, eastern Guadeloupe and Anguilla) (Budd et al., 1995; Cornée et al., 2012; Münch et al., 2013). Perched turbiditic basins surround these reliefs (Bouysse and Mascle, 1994; De Min et al., 2015). North of Guadeloupe, the trench-parallel Kalinago Basin separates the remnant arc islands from the present-day volcanic arc. Along the latter, series of arc-parallel, en-échelon, deep basins are interpreted as right-stepping transtensive relays for an incipient strike-slip structure possibly related to strain partitioning (Feuillet et al., 2011; Feuillet et al., 2002; Laurencin et al., 2019). However, evidences of their sedimentary architecture and tectonic deformation are lacking and impede to progress on the understanding of their origin and evolution along with the margin bending.

3 Data Acquisition and Processing

3.1 Multi-Channel Seismic (MCS)

Over the northernmost features of the NLA V-shaped Basins-and-Spurs System located offshore St Barthelemy and Barbuda islands, we present 5 of the 54 MCS lines acquired during cruises ANTITHESIS 1 and 3: 3 dip lines (Ant06, 14, 40) and 2 associated strike lines (Ant38.2, 42). Along MCS line Ant06, Wide Angle Seismic data were also recorded (Laurencin et al., 2018). The low frequency (~20 Hz) MCS acquisition parameters are summarized in

Table 1. Pre-processing (Quality control and 12.5 meters binning) were performed onboard using QCSispeed® and SolidQC® software's (Ifremer). We conducted post-processing with Geovation® (CGG) following a processing sequence that include:

- Additional gain function of time to correct the spherical divergence
- 2 phases of high amplitude and low frequency noise attenuation
- External mute on shot point to remove direct and refracted waves
- Iterative stacking-velocity analysis: 1 on stacked sections and 3 on Common Middle Point
- Normal Move-Out (NMO) using the final velocity law
- External mute after NMO to reduce far offset stretching
- Multiple attenuation with 2D-SRME method (Adaptive Surface-Related Multiple Elimination: Multiple modeling and adaptive subtraction of the multiple model from data (Verschuur et al., 1992).
- Predictive deconvolution to improve data resolution

- Internal mute on gathered CMP to remove the short offsets of residual multiples
- Second phase of multiple attenuation in Radon domain
- Stack with a time variant Band-Pass filter (3,5,70,80 Hz from 0 to 6s and 3,5,35,45 Hz from 8 to 15s)
- Post-stack (f,k) migration at constant velocity (1500 m/s) and BP filter (3,5,70,80 Hz)

We applied an additional Automatic Gain Control (AGC) with a large 1.5 s gate to improve the signal at high depth without degrading reflections contrast in order to improve the printed section quality.

3.2 Multibeam swap bathymetry

We acquired bathymetric data with a Kronsberg EM-122 and a Reson Seabat 7150 multibeam echosounders onboard R/V *L'Atalante* and R/V *Pourquoi Pas?* respectively. We complemented the dataset with other French cruises multibeam data including SISMANTILLES 2 (Laigle et al., 2007), KASHALLOW 2 (Lebrun, 2009) and AGUADOMAR (Deplus, 1998) cruises. Multibeam spatial resolution depends on aperture and number of beams of the echosounders, shooting rate and ship speed (5 kt during MCS acquisition or 10 kt) and thus varies greatly with depth. Given the wide range of depth in our area, we produce sounding density maps to determine an optimal DTM grid spacing at 75 m. This ensures sufficient sounding averaging for each DTM cell (min. ca. 5 sounds) and allows reducing the interpolation down to 2 rows, to ensure a total coverage even in areas of great depth. Vertical resolution is also depth dependent, and ranges from a few decimeters at shallow depth to tens of meters at great depth. Data processing, performed with Caraïbes® and Globe® software, consists in removing aberrant probes, near neighbor DTM gridding and filtering. We generated high-resolution bathymetric slopes and slope directional maps using QGis® software for morpho-structural interpretations purpose and illustrations.

4 Results

4.1 Morpho-structure of the NLA Margin

At the NLA subduction zone, to the east of the deformation front, numerous seamounts, bending faults and elongated ridges of the oceanic fabric along with a very thin sedimentary fill roughen the seafloor of the up-to-8000-m-deep subducting plate (Figure 1 and Figure 3A). To the west, a ~30-km-wide accretionary wedge (yellow zone in Figure 3B) with a classical morphology of an in-sequence fold and thrust belt extends to the Bunce Fault (i.e. the margin

backstop). The outer forearc (white zone in Figure 3B) extends from the Bunce Fault to the slope break and consists in >4500-m-deep flat basins to the northwest of 18.6°N and 61.8°W (dotted pattern in Figure 3B) and in a more elevated seafloor showing N320-350°-trending sigmoid lineaments, to the southeast. The inner forearc (grey zone in Figure 3B) shows a north-south sequence of basins and spurs from the Anegada Passage to the Karukera Spur (Figure 2). N70°-N90°- and N20°-N50°-trending linear scarps structure the southern and northern flanks of the basins, respectively, resulting in their V shape (blue lines in Figure 3B). The southeastern flank is usually steeper suggesting that these asymmetric basins are mainly controlled by northwestward-dipping faults. These V-shaped basins narrow and terminate eastward of the remnant arc islands that stand in the NLA Forearc. The smooth basins floor gently dips trenchward, contrasting with the rough spurs seafloor and the outer forearc topography (Figure 2).

To the south, the subducting and southward sweeping Barracuda Ridge deforms the accretionary wedge, the outer forearc and the trenchward part of the V-shaped basins (Figure 2). For instance, La Désirade Basin gently dips and opens toward the outer forearc to the south of the deformed area, while uplifted and inverted basins front La Méduse Basin located above the subducting ridge. At the open side of La Désirade Basin, fault-bounded basement highs and associated linear N50-60°-trending bathymetric ridges extend from the Bertrand and Falmouth Spurs (Figure 2) (see seismic line SL3, Figure 3 in Laigle et al., 2013). To the north, the outer slope of the Antigua, Barbuda, St Barthelemy and Anguilla Valleys is steep and truncated by trench-parallel escarpment. The seafloor morphology and deep seismic images recorded in and around the St Barthelemy Basin provides evidences about the geological evolution of these V-Shaped basins.

4.2 Morpho-structure of the St Barthelemy Valley and surrounding spurs.

The up-to-70-km-wide V-shaped St Barthelemy Valley separates the >80-km-long, >20-km-wide NE-SW-trending Tintamare Spur to the north from ~60-km-wide Barbuda Spur to the south (Figure 3). The spurs crest climaxes 3600-4000 m above the 3500-5700m-deep and 1.5°-trenchward-dipping smooth seafloor of the St Barthelemy Valley. Some canyons, running from the carbonate platform (Figure 3A) to small deltaic mass-deposits, incise the spurs flanks (Figure 3). From south to north, three sets of trench-facing escarpments, up-to-100-m-high (red, orange and yellow in Figure 3B) define a ~1000-m-high drop toward the outer forearc. First, in the Antigua Basin (Figure 3A) immediately north of the subducting Barracuda Ridge, the escarpments trend N340° (red in Figure 3B). Second, northward, N300°-trending

escarpments (orange in Figure 3B), extend along a 30-to-40-km-wide zone which spreads from the outer forearc in the East through the Saint Barthelemy and Anguilla Valleys, and the Barbuda and Tintamarre Spurs. Third, to the north, at the Anguilla Valley (Figure 3A), N280°-trending escarpment (yellow in Figure 3B) truncate the N300°-trending escarpments. This latter escarpment set extends from the outer forearc to the Sombrero Basin (Figure 2), sub-parallel to the left-lateral strikes-slip Maliwana-Sombrero System (Laurencin et al., 2017) (Figure 3). These three sets of trench-facing escarpments truncate and locally vertically offset the scarps that bound the spurs and the basins without systematically offsetting them laterally. They are directed N340°, N300° and N280° from south to north, indicating a 60° counterclockwise rotation of the forearc fracturing, which is consistent with an accommodation of the trench-parallel increase of the margin convex geometry.

4.3 Tectonic and stratigraphic architecture of the NLA margin

In the following section we decipher the stratigraphic architecture and tectonic features along the St Barthelemy Valley, the N-Barbuda and Tintamarre Spurs, based on dip MCS lines Ant06, 14, 40 and on strike MCS line Ant38.2, 42 (Supplementary Material and Figure 4).

4.3.1 The subducting plate

The subducting oceanic crust shows faint and irregular reflectors floored by series of short irregular low frequency reflectors at Moho depth, derived from wide-angle model along line An06 (Klingelhoefer et al., 2018; Laurencin et al., 2018). The strong amplitude low frequency reflectors at the top of the oceanic crust in the trench progressively faint beneath the outer forearc and vanishe beneath the tip of the inner forearc. Subducting horsts and grabens roughen the top of the crust consistently with the seafloor morphology to the east of the trench. The decollement corresponds with irregular, average amplitude, low frequency reflectors with locally reverse polarity. The top of the oceanic crust and the decollement encompass low amplitude sub-parallel reflectors in the subduction channel revealing a thin section of preserved poorly deformed subducting sediments, mainly located in the grabens (Figure 4 and Supplementary Material).

4.3.2 The upper plate basement

Wide-angle model Ant06 shows that the Moho of the upper plate dips landward from 23 to 28 km depth (Klingelhoefer et al., 2018; Laurencin et al., 2018). At this depth, low amplitude, low frequency, discontinuous reflectors rise slowly from 13 stwt at CDP 7750 to 10 stwt at

CDP 14000 as a result of pull up effect (Supplementary Material and Figure 4). Line Ant40, shows similar reflections from 13 to 12 stwt at CDP 500-3000. Upward, the poorly reflective basement shows locally low frequency, low amplitude, irregular to chaotic reflectors. Vertical velocity gradient in the basement, derived from wide-angle data, is characteristic of an arc igneous crust (Klingelhoefer et al., 2018; Laurencin et al., 2018). Strong amplitude and low frequency series of reflectors, *UB0*, separate the basement from the overlying stratified sedimentary units.

Average amplitude and frequency, sub-parallel rather continuous landward dipping reflectors define a wedge-shaped unit beneath the outer forearc, immediately west of the Bunce Fault, at CDP 3700–6000 in line Ant06 and at CDP 7000–5500 in line Ant40. This unit rests above the decollement and beneath the margin basement. Above this wedge, the top of the margin basement *UB0* turns from trenchward dipping to landward dipping. This wedge-shaped unit doesn't exist along the line Ant14 (Supplementary Material and Figure 4) and the margin basement topography continuously dips trenchward while the basement crust thins. Similar structure is also described offshore of the Karukera Spur beneath the outer forearc (Bangs et al., 2003, Evain, 2013 #579; Laigle et al., 2013). The transpressive positive flower structure of the Bunce Fault bounds the margin basement trenchward (Laurencin et al., 2019). To the east, series of arcward dipping, continuous and high frequency reflectors indicate and imbricated structure of in-sequence thrusts within an accretionary prism.

4.3.3 The margin slope basins stratigraphy

Based on sismo-stratigraphic description, we define 4 sedimentary units, *U1* to *U4*, above the basement unconformity, *UB0*, separated by 3 unit boundaries, *UB1* to *UB3*. The most complete sequence is preserved in the St Barthelemy Valley as revealed by lines Ant40 and Ant38.2-42 (Supplementary Material and Figure 4).

At the bottom of the St Barthelemy Valley, deep reflectors of unit *U1* lap onto *UB0* toward the arc and the spur flanks. *UB1* conformably tops *U1* albeit local truncations in the thickest and faulted part of the basin. Onlaps of unit *U2* reflectors onto *UB1* help at identifying this unconformity. *U1* reflectors are low-frequency, low-amplitude, layered and continuous upslope and more discontinuous and poorly-layered in the basin. *U1* is up-to-1stwt-thick in contact with the basin bounding faults (Ant40 CDP 2750-3500; Ant42 CDP 200-2000) and thins above buried horsts (Ant42 CDP 500-1000).

In the St Barthelemy Valley, trenchward-dipping unit *U2* rests unconformably above *UB1*, retrograding landward with onlaps above *UB0* over the spurs and the upper margin plateau. Strike line Ant38.2-42 shows that *U2* reflectors downlap onto *UB1* in the valley, indicating a

progradation from the spurs to the basin centers. Strong amplitude reflector *UB2* tops *U2* with numerous reflector truncations, which classically indicate erosional surfaces. *U2* shows average amplitude, average frequency, layered discontinuous to irregular reflectors upslope and lower amplitude, higher frequency and more chaotic reflectors above the outer forearc. Over the spurs, *U2* is 1-1.5-stwt-thick with local variations controlled by incisions and fan-shaped deposits at fault bounded basins (at CDP 9000-10000 in line Ant06 for instance). *U2* thickens up to ~2.5 stwt in the eastern part of the St Barthelemy Valley (CDP 1875 in line Ant38.2-42). The steeply dipping and downlaping reflectors of *U2* result in an overall fan shape located near faults that dip from the Tintamarre Spur toward the basin.

Unit *U3* is located over the uppermost plateau, the Barbuda Spur slope (Ant06) the St Barthelemy and Barbuda Valleys (Ant38.2-42) but is absent over the outer forearc and the Tintamarre Spur (Ant14). Deep *U3* reflectors lap onto *UB2* at the upper plateau. In contrast, in the valley, these reflectors show downlaps onto *UB2* in the dip direction and onlaps in the strike direction revealing a trenchward prograding unit. *UB3* tops *U3*, mostly conformably at the plateau but truncating uppermost reflectors in the St Barthelemy and Barbuda Valleys. The high frequency and average amplitude reflectors of *U3* are layered and continuous over the plateau and more irregular in the valleys. This unit thickens from the plateau to the valley, up to 0.9-stwt at the valley center (Ant40 CDP 3250, Ant42 CDP 1200), forming fan shapes at southeast dipping faults.

Unit *U4* is up-to-0,4-stwt-thick in local narrow residual basins along the upper slope plateau (Ant06 CDP 12000-14600) and in the deep outer forearc basin (Ant14 CDP 4000-6200) where it rests unconformably upon *UB2*. Deep reflectors of *U4* downlap trenchward onto *UB2* at the outer forearc (Ant06 and Ant40) and onlap onto *UB3*, landward into the valleys. *U4* reflectors are irregular and poorly layered over the outer forearc and more continuous upslope with high frequency and average amplitude. *U4* shows fan-shaped deposits, perpendicular to the basin axis (line Ant38.2-42) that progressively infill the valleys retrograding onto the basin border faults.

4.3.4 Tectonic deformation in the Basins-and-Spurs System

Based on bathymetric morphostructures and deep seismic images, we identified two main sets of faults. N40-90°-trending faults bound the V-shaped basins, dipping toward the basin axis (blue lines in map, Figure 3B and in strike lines Ant38.2-42, Figure 4). The N300° trending Tintamarre Faults System (Orange lineaments in Figure 3 and dip lines Ant06, Ant40 and Ant14, Figure 4) crosscuts the basins and the spurs (Figure 5).

The St Barthelemy Valley is an asymmetric graben between two spurs. At the basin northern flank, in the hanging wall the basement is downwardly offset by southeastward-dipping listric normal faults (planes A, B, C at CDP 2000-2300 in line Ant38.2 and CDP 900 in line Ant42 – Supplementary material and Figure 4). *U1* and *U2* show fan shape in the basin associated to these faults. At the southern bound of the basin, steeper northwestward-dipping normal fault planes D, E (line Ant38.2-42 CDP 2250-2900) also dip toward the basin axis. Most of these normal and listric faults are deeply rooted, possibly soling out downward onto the interplate contact. This crustal-scale fracturing shift downward the basement top, *UB0*, by 4.5-stwt, from 7 stwt at the Tintamarre Spur crest, to 11,5 stwt at the deepest point in St Barthelemy Valley (line Ant38.2-42). Considering P-waves velocity of 1500m/s in the water and ~2500m/s in the sediments, the vertical drowning of the basin floor is up to ~5000m. At last, tectonic restoration allows estimating the amount of extension across the mouth of the V-shaped basin to be ~20%, which is consistent with the bulk crustal extension estimates provided by Legendre et al. (2018).

U1, restricted to the St Barthelemy Valley, is thicker in the grabens than over the horsts revealing a syntectonic deposit during the opening V-shaped basin. The drastic increase in sediment thickness in the valley is mainly accommodated by *U2* thickening. This thickening associated to fan-shaped reflectors series dipping and prograding toward the basin axis are likely to be related to N40°-90°-trending faults activity. *U3* is mostly horizontal showing locally smaller fan-shapes against the valleys bounding faults. Some of these faults seal into *U2* (at CDP 1500 in line Ant-40 for instance), while others remain active up to *U3* (at CDP 1000 in line Ant38.2-42) and seal before *U4*. Thus, tectonic activity at the N40-90° valley-bounding faults initiates during *U1*, climaxes during *U2* and progressively ceased during early deposits of *U3* (Figure 6). Any present-day activity for these faults is uncertain and/or of second order as revealed by the systematic offset of the surface traces of the N40°-90° faults by the N300° faults in map view (Figure 3).

The N300°-trending, up-to-100m-high scarps across the Basins-and-Spurs System correspond at depth with steep, trenchward-dipping normal faults. This Tintamarre Faults Zone controls landward tilted basins and trenchward drowned crustal blocs in their hanging walls. These faults offset the seafloor and affect the thickness of recent sedimentary units U3 and U4 indicating a recent syn-sedimentary tectonic activity. These faults are deeply rooted, possibly down to the interplate contact (at CDP 3000-4000 in line Ant40 and CDP 7000-7500 in line Ant06) or down to intracrustal layered reflectors (~12-stwt-dip in line Ant40 CDP 2000-2500 and ~10-stwt in line Ant06 CDP 8500-10000) the Moho being substantiated at >13-stwt-depth based on wide-angle seismic data. Although deciphering the faulting initiation is

hazardous, the N300° faults systematically offsets the N40°-90° faults indicating that Tintamarre faults activity postdates that of the Spur-bounding faults (Figure 6).

We conclude that two main sets of faults affect the NLA inner forearc domain and that the two fault systems were successively active through time (Figure 6). First, a N130°-160° directed (trench-parallel) extension controlled the V-Shape fracturing of the basins during *U1* and *U2* deposition. Then, a N10-30° directed (trench-perpendicular) extension generated normal faulting sub-parallel to the trench during *U3* and *U4* deposition. This latter fault system accommodates the regional forearc subsidence and basement thinning.

5 Tectonic evolution of the NLA forearc

As discussed in the following, we interpret two successive extensive tectonic phases in the NLA forearc separated by a regional emersion, the *UB2* unconformity. Prior to the emersion phase, trench-parallel extension triggered crustal normal faulting that opened the transverse V-Shaped valleys. Since *UB2*, trench-perpendicular extension generated ~50-km-wide, >300-km-long N300°-trending Tintamarre Faults Zone associated with basement thinning and long-lasting margin subsidence.

5.1 Regional emersion phases

The widespread unconformity, *UB2*, separates deep deformed, tilted sedimentary units thickening toward the basin axis with local syn-tectonic features, from overlying units of less deformed reflectors draping unconformably at low angle over *UB2.* This unconformity shows widespread high-angle truncations on top of *U2* and incisions, from the outer forearc to the upper slope, which indicate a regional erosion surface during a subaerial to shallow water phase. This large-scale uplift and emersion phase indicates a major tectonic rearrangement before a drowning to great depth. Stratigraphic correlations, discussed in the following, suggest an earliest mid Miocene age for *UB2*.

To the west, at the Saba Bank, two unconformities are observed in SB2 well, Oil company MCS lines (Church and Allison, 2004) and lines GA15B-C-GA08 (Figure 7) recorded during the GARANTI cruise (Lebrun and Lallemand, 2017; Philippon et al., 2019). From Church and Allison (2004), a late Eocene unconformity *S3* separates an undrilled basement unit topped by mid Priabonian andesitic lavas flows overlaid by a very late Eocene to early Oligocene Lower Carbonate and Turbiditic unit. The latter is topped by an erosional unconformity *S4*, overlaid by a late Oligocene to early Miocene Fluvial deltaic unit. This latter is crosscut at top by an erosional unconformity *S5* which dates to the earliest mid Miocene. These features

indicate shallow waters and emersion phases. An earliest mid Miocene erosional unconformity is also found onshore in the Anguilla Bank. There, mid Miocene sediments are missing in Saint Martin island and the unconformity laterally correlates to an erosional unconformity overlain by Langhian Megabreccia deposits in nearby Tintamarre Islet (Andreieff et al., 1988; Léticée et al., 2019). This earliest mid Miocene unconformity is of regional extent as it was found offshore into the Kalinago Basin to the Saba Bank (Cornée et al., 2019). Farther South, at the latitude of Guadeloupe island, Bouysse and Mascle (1994) interpreted an early Miocene unconformity between deep complex sedimentary sequences and an onlapping sedimentary cover, which has been subsiding trenchward by more than 2500m. Consistently, at the Karukera Spur, a prominent unconformity on top of an early Miocene shallow water carbonate platform subsequently subsided and tilted trenchward leading to basinal environment deposit during the mid Miocene (De Min et al., 2015). Consequently, our subaerial erosional unconformity *UB2* likely corresponds to the earliest mid Miocene unconformity extending over the northern Lesser Antilles forearc and backarc, below latest mid Miocene to Pliocene deposits. This unconformity indicates a regional-scale earliest mid Miocene emersion phase in the NLA forearc, possibly slightly diachronous north to south from our study area to the latitude of Guadeloupe island.

A lower boundary age for *U1* can be proposed. At St Barthélemy and in the backarc, compressional tectonic structures are sealed by a late Priabonian unconformity (Church and Allison, 2004; Philippon et al., 2019). Following this compression, the Kalinago Basin opening and extensive evidences in the northern Anguilla Bank attest for a regional extension during the early Oligocene (Cornée et al., 2019; Legendre et al., 2018). Syntectonic deposits of Unit *U1* in the Saint-Barthelemy Valley suggest that the oldest sediments in the V-shaped basin postdates the late Priabonian unconformity. Thus, *U1* and *U2* are likely to be Oligocene – Early Miocene, partly synchronous with the opening of the Kalinago Basin.

The collision and oblique subduction of the southeastern extension of the Bahamas Bank at the Northeastern Caribbean Plate started at the late Eocene and has progressively swept westward during the Miocene (Leroy et al., 2000; Pindell and Kennan, 2009). Along the PRVI Margin Segment, the emersion phase is interpreted as the tectonic consequence of the obliquely subducting and westward sweeping southeastern extension of the Bahamas Province (Grindlay et al., 2005). We do not rule out this subduction influence onto the Greater Antilles tectonics, but it is unlikely that the overthickened crust of the Bahamas Province extended beneath the Lesser Antilles as far south as the Karukera Spur. Alternately, mechanical modelling shows that at convex convergent margin, the subduction focus strain toward the convexity axis, generating uplift in the forearc area (Bonnardot et al., 2008). These models conclude that the subduction bending into convex shape causes these vertical motions. Thus, subduction at the convex Northeastern Caribbean Margin possibly generated

similar effect resulting in a regional uplift in the NLA forearc that lead to the regional emersion recorded during the earliest mid Miocene.

5.2 Margin bending and V-Shaped valleys

Interpreted seismo-stratigraphic correlations suggest that the tectonic activity of the N40-90°-trending faults, bounding the spurs and V-shaped valleys, started during unit *U1*, topped by unconformity *UB1*, estimated to be Oligocene, and climaxes during unit *U2*, before erosional surface *UB2* which is estimated to be earliest mid Miocene.

Since the Paleocene–early Eocene time, the collision and oblique subduction of the southeastern extension of the Bahamas Bank has progressively swept westward along the Caribbean Plate (Figure 8) generating an increase in the NLA margin convexity. The consecutive Margin bending likely generated counterclockwise block rotations. The margin has recorded a rotation of 25° in Puerto-Rico (Calais et al., 2016; Mann et al., 2002; Mann et al., 2005; Reid et al., 1991) and 15° to 25° in St Barthelemy (Philippon et al., 2020) since the end of the Oligocene. Backarc tectonic shortening in the Saba Bank and at St Barthelemy island indicating trench sub-perpendicular tectonic compression ceased by the end of the Eocene (Philippon et al., 2020). Subsequently, Oligocene - early Miocene extension and subsidence in the Kalinago basin resulted, at least partly, from the activity of NW-SE and ENE-WSW extensive faults systems bounding the basin and the Anguilla Bank, respectively (Cornée et al., 2019). Moreover, the margin convex bending implied N-S to NW-SE extension in the forearc domain (Jany et al., 1990; Masson and Scanlon, 1991). Consistently, deep seismic images indicate that the opening of the Sombrero and Malliwana basins was triggered by an old, currently sealed, NW-SE extensive tectonic phase (Laurencin et al., 2017). This trench-parallel extension is consistent with N40-90° normal fracturing observed at the scale of the forearc domain. Thus, the V-shaped valleys opening, during the Oligocene, is likely to be related to the increasing margin convexity following the Bahamas Bank collision.

Feuillet et al (2002, 2011) proposed that northward increasing amount of plate motion partitioning along a curved subduction zone generated the V-Shaped basins within a lithospheric forearc sliver bounded by a left-lateral major strike-slip system along the arc. However, no large amount of lateral motion is expected along the incipient en-échelon normal fault system in the arc (Laurencin et al., 2019). Moreover, these V-shaped basins mostly open at the Oligocene, when the subduction zone was more linear and thus less prone to plate motion partitioning. Thus, deep seismic images presented in this study rule out the tectonic model of a major control onto NE-SW faults activity and V-shaped Valleys opening by strain partitioning in the NLA Forearc.

As a result, we propose that, during Oligocene time, the NLA forearc accommodated the margin convex bending by trench-parallel extension along N40-90°-trending normal faults which controlled the opening of the V-shaped valleys (Figure 8). By the mid-Miocene, Anegada Passage tectonics dissociated the PRVI margin segment from the NLA. Plates interaction at the convex subduction zone triggered a regional emersion all along the NLA Margin from the Sombrero Basin to the Karukera Spur.

5.3 Forearc subsidence, basal erosion and volcanic arc migration.

The earliest mid Miocene sub-aerial unconformity *UB2* is currently located up-to-7-stwt-deep in margin slope basins suggesting dramatic forearc subsidence, estimated to be up-to-340 m/Myr, since the mid-Miocene (~16Ma). Consistently, to the south, offshore of Guadeloupe Island, large-scale margin subsidence at the Karukera Spur results in significant trenchward tilting of the inner forearc domain (De Min et al., 2015). To the northwest, the PRVI Margin segment has recorded a subsidence greater than 3.2 km since the Pliocene, following subduction of the buoyant ~20-km-thick southeastern tip of the Bahamas Province (Grindlay et al., 2005).

At the NLA, the Tintamarre Fault Zone (Orange lines in figure 3B) is associated with a major basement thinning (Figure 4 and Supplementary Material). Wide-angle-derived Velocity Vp in the basement ranges from 4.5 km/s to 7.3 km/s from top to bottom in line Ant06 (Klingelhoefer et al., 2018; Laurencin et al., 2018). Based on this velocity, we estimate that the crustal thickness decreases from ~14.75 km landward from the fault zone to ~7.7 km at the hanging wall and increases again to ~10.7 km trenchward from the fault, in 20 km distance from CDP 6400 to 8000 (Figure 4). Similar calculation in line Ant40, from CDP 2400 to 4300, results in estimating a crustal thinning from ~14.6 km and ~10.1 km landward and seaward of the fault zone respectively to a minimum of ~5.3 km at the fault zone axis (Figure 4 and Supplementary material). Thus, along the fault zone, the basement thickness is reduced by 28-48% compared to the outer forearc trenchward and by 48-64% compared to inner forearc arcward. Although extrapolating any ante-extension basement thickness at the fault zone is uncertain, we can reasonably estimate an up-to-50% crustal thinning. Therefore, forearc extension and thinning, notably along the Tintamarre Fault Zone, is likely to participate to the Neogene regional subsidence.

At numerous erosive margins, subduction-erosion beneath the margin slope is inferred from long-term subsidence and tilting, regional tectonic extension and disrupted topography in the wake of subducting seafloor rugosity and relief (e.g. Clift and Vannucchi, 2004).

Moreover, fluids, driven downward into the subduction channel and the subducting plate, then expelled upward at depth to the margin toe, favor margin basal hydrofracturing and erosion (von Huene et al., 2004). As a result, high subsidence rates, with significant variations through times, are typical for erosional margins. This rate is estimated to be locally up-to-600 m/Myr at the middle America Trench for instance (Vannucchi et al., 2004). At the NLA Trench, the oceanic crust, originated from the slow mid-Atlantic Ridge shows a rough topography, subducting major oceanic transform fault zones and a thin sedimentary fill, which favor pervasive crust hydration and mantle rocks serpentinization (e.g. Grevemeyer et al., 2018). Moreover, the Tintamarre fault zone is associated with wide-angle-derived velocity anomalies in the basement and the sediment (Klingelhoefer et al., 2018) and anomalously high heat flow in surface (Biari et al., 2017). These authors interpret these anomalies as the result of warm fluids upward migration through the faulted forearc crust. Major deeply-rooted faults systems in forearc are prone to channelize fluids from the plate interface to the seafloor favoring basal hydrofracturing (von Huene et al., 2004), forearc subsidence (Contreras-Reyes et al., 2014) and slope sediment destabilization (Hensen et al., 2004). As a result, at the NLA, post mid-Miocene geodynamical and tectonic context favors NE-SW margin extension, fluid migration and consequently basal tectonic erosion and forearc subsidence.

Moreover, the volcanic activity ceased along the remnant lesser Antilles Arc during the earliest Miocene (Legendre et al., 2018) and resumed ~50km landward during the early Zanclean along the present-day arc (Lindsay et al., 2005) implying a volcanic arc retreat rate of ~2 to 5km/Myr. Various investigations (e.g. Allen et al., 2019; Bouysse and Westercamp, 1990) suggest that a slab shallowing triggered this arc landward migration without resolving the question of the causes for this shallowing. At the PRVI Margin, landward migration of the trench-slope break, associated to forearc subsidence, is possibly related to the subduction of the southeastern tip of the buoyant Bahamas Bank (Grindlay et al., 2005). However, it is very unlikely that the bank subducted underneath the NLA as far south as the latitude of Guadeloupe. Moreover, the bank has been subducting since the late Eocene and was drifting away westward by the late Miocene – Pliocene times. At last, the post mid-Miocene regional drastic forearc subsidence is poorly consistent with a slab shallowing able to generate a 50km landward arc retreat. In contrast, the geographically and chronologically consistency between the arc retreat and the forearc subsidence suggests that this retreat is mainly controlled by margin tectonic erosion. Such erosion-related arc migration was described at various subduction zones, as first documented in Tonga (Pelletier and Dupont, 1990), Peru and Japan (von Huene and Lallemand, 1990) for instance. One would object that a 50km migration would requires a surprisingly efficient basal erosion, considering the slow convergence rate at the Lesser Antilles Margin. The subducting plate rugosity drastically increases to the north of the

Tiburon and Barracuda Ridges as the trench fill thickness decreases from >7km at 11°N (Westbrook et al., 1984) to <500m at 17°N (Laigle et al., 2013; Laurencin et al., 2017; Pichot et al., 2012). Simultaneously, the width of the accretionary prism decreases, from south to north of the ridges, from >100km (Deville and Mascle, 2012; Westbrook et al., 1984) to 30km (Laurencin et al., 2019). The South-American Orinoco and Amazon rivers are the main source of sediments in the abyssal province (Wright, 1984) and their northward transport by the strong Antarctic Bottom Water current (AABW) is interrupted by the Tiburon and Barracuda Reliefs (Embley and Langseth, 1977). Various authors estimate that these Ridges start interacting with the NLA trench at the late Miocene - early Pliocene (e.g. McCann and Sykes, 1984; Pichot et al., 2012). We postulate that, by this time, the oceanic plate features generated vigorous tectonic erosion of the NLA margin to the north of the ridges. Subduction of an old, sediment-starved, rough, fractured, hydrated, serpentinized oceanic basement possibly interrupted the previously rather continuous accretionary regime, triggered drastic frontal erosion of the prism and enhanced fluid release at depth, generating upper-plate hydrofracturing and basal erosion. Such drastic erosion is likely to result in forearc subsidence associated with westward migration of the deformation front and the volcanic arc.

Conclusion

Numerous examples of subduction zones in the world undergo tectonic impact of buoyant province collision, including large-scale blocks rotation, plate boundary curvature, backarc rifting and tectonic escape. Investigating the Northern Lesser Antilles subduction zone sheds new light onto the margin polyphased tectonic evolution that accommodated increasing margin convexity in a context of along-strike transition from subduction to collision.

Based on interpreted high-resolution bathymetric, MCS and WAS data acquired during ANTITHESIS and GARANTI cruises in the NLA forearc, we identify two main tectonic phases separated by a regional-scale emersion period.

During the Eocene - Oligocene, the Bahamas Bank subduction/collision with the northeastern boundary of the Caribbean Plate has generated progressive bending of the margin into the current convex geometry. Resulting trench-parallel tectonic extension is accommodated, at least partly, along N40-90° normal faults, that bound V-Shaped valleys at the inner forearc. The origin of this prominent NE-SW fracturing in the forearc is thus very unlikely to be related to current strain partitioning. This bending resulted in a regional margin uplift and emersion phases at the early-mid-Miocene.

Since mid-Miocene, the forearc has recorded regional subsidence and tectonic extension, at least partly accommodated along the N300° Tintamarre normal Faults Zone. This tectonic phase reveal drastic margin basal and frontal tectonic erosion, which has likely generated westward migration of the deformation front and the volcanic arc since the mid Miocene.

The Antithesis and Garanti cruise teams include:

Agranier, A., Arcay, D., Audemard, F, Beslier, M.-O., Boucard, M., Bouquerel, H., Conin, M., Cornée, J.J., Crozon, J., Dellong, D., De Min, L., de Voogd, B., Evain, M., Fabre, M., Gay, A., Graindorge, D., Gwandai, W., Heuret, A., Klingelhoefer, F., Laigle, M., Lallemand, S., Laurencin, M., Lebrun, J.-F., Legendre, L., Léticée, J.L., Lucazeau, F., Mahamat, H., Malengros, D., Marcaillou, B., Mazabraud, Y., Mercier de Lepinay, B., Olliot, E., Oregioni, D., Padron, C., Pichot, T., Prunier, C., Quillévéré, F., Ratzov, G., Renouard, A., Rolandonne, F., Rousset, D., Schenini, L., Thomas, Y., Vitard, C., Yates, B.

Acknowledgments

We acknowledge ANTITHESIS, SISMANTILLES and GARANTI scientific and technical teams on board R/Vs *L'Atalante* and *Pourquoi-Pas?* for high quality data acquisition and processing. We are grateful to the regional council of Guadeloupe that provided Milton Boucard thesis funding. This work is also part of the French ANR17-CE31-0009 GAARANTI program. Multichannel processing has been done with Geocluster software of CGG and with Seismic Unix for the figures. Most of the figures were drafted using GMT, Qgis, and Adobe Illustrator software.

Every geophysical data of the Antithesis cruises is available on the internet site of the French Oceanographic Fleet (https://campagnes.flotteoceanographique.fr/search). Interested readers select the "Antithesis" campaign and the desired dataset in field "Data Managed by SISMER". Once every needed dataset is selected, the readers can send a request form from "My basket" page.

References

Allen, R.W., Collier, J.S., Stewart, A.G., Henstock, T., Goes, S., Rietbrock, A., 2019. The role of arc migration in the development of the Lesser Antilles: A new tectonic model for the Cenozoic evolution of the eastern Caribbean. Geology 47, 891–895, doi:10.1130/G46708.1.

Andreieff, P., Westercamp, D., Garrabé, F., Bonneton, J.-R., Dagain, J., 1988. Stratigraphie de l'île de Saint Martin (Petites Antilles Septentrionales). Géologie de la France 2-3, 71-88.

Angelier, J., 1978. Tectonic evolution of the Hellenic Arc since the late Miocene. Tectonophysics 49, 23-36, doi:10.1016/0040-1951(78)90096-3.

Bangs, N.L.B., Christeson, G.L., Shipley, T.H., 2003. Structure of the Lesser Antilles subduction zone backstop and its role in a large accretionary system. J. geophys.Res. 108, 2358, doi:10.1029/2002JB002040.

Biari, Y., Marcaillou, B., Klingelhoefer, F., Lucazeau, F., Rolandone, F., Heuret, A., Pichot, T., Bouquerel, H., 2017. Thermal regime along the Antilles subduction zone: Influence of the oceanic lithosphere materials subducted in the oceanic crust. EGU General Assembly Vienna, 19, EGU2017-15003, 24-28/04/2017, https://meetingorganizer.copernicus.org/EGU2017/EGU2017-15003.pdf.

Bonnardot, M.A., Hassani, R., Tric, E., Ruellan, E., Régnier, M., 2008. Effect of margin curvature on plate deformation in a 3-D numerical model of subduction zones. Geophys. J. Int. 173, 1084-1094, doi:10.1111/j.1365-246X.2008.03752.x.

Boschman, L.M., van Hinsbergen, D.J.J., Torsvik, T.H., Spakman, W., Pindell, J.L., 2014. Kinematic reconstruction of the Caribbean region since the Early Jurassic. Earth-Science Reviews 138, 102-136, doi:10.1016/j.earscirev.2014.08.007.

Boutelier, D.A., Cruden, A.R., 2013. Slab rollback rate and trench curvature controlled by arc deformation. Geology 41, 911-914, doi:10.1130/g34338.1.

Bouysse, P., Andreieff, P., Richards, M.A., Baubron, J.C., Mascle, A., Maury, R.C., Westercamp, D., 1985. Aves swell and Northern Lesser Antilles Ridge: Rock-dredging results from Arcante 3 cruise. Géodynamique des Caraïbes, symposium Paris, 65-76.

Bouysse, P., Mascle, A., 1994. Sedimentary basins and petroleum plays around the French Antilles, in: Mascle, A. (Ed.), Hydrocarbon and petroleum geology of France , special publication of the EAPG. Springer-Verlag, pp. 431-443.

Bouysse, P., Westercamp, D., 1990. Subduction of Atlantic aseismic ridges and Late Cenozoic evolution of the Lesser Antilles island arc. Tectonophysics 175, 349-380, doi:10.1016/0040-1951(90)90180-G.

Budd, A.F., Johnson, K.G., Edwards, J.C., 1995. Caribbean reef coral diversity during the early to middle Miocene: an example from the Anguilla Formation. Coral Reefs 14, 109-117.

Calais, E., Symithe, S., Mercier de Lépinay, B., Prépetit, C., 2016. Plate boundary segmentation in the northeastern Caribbean from geodetic measurements and Neogene geological observations. Comptes Rendus Geoscience 348, 42-51, doi:10.1016/j.crte.2015.10.007.

Church, R.E., Allison, K.R., 2004. The Petroleum Potential of the Saba Bank Area, Netherlands Antilles.

Clift, P.D., Vannucchi, P., 2004. Controls on tectonic accretion versus erosion in subduction zones: Implications for the origin and recycling of the continental crust. Reviews of Geophysics 42, RG2001, doi:10.1029/2003RG000127.

Contreras-Reyes, E., Becerra, J., Kopp, H., Reichert, C., Díaz-Naveas, J., 2014. Seismic structure of the north-central Chilean convergent margin: Subduction erosion of a paleomagmatic arc. Geophysical Research Letters 41, 1523-1529, doi:10.1002/2013gl058729.

Cornée, J.-J., BouDagher-Fadel, M., Philippon, M., Léticée, J.-L., Legendre, L., Maincent, G., Lebrun, J.-F., Münch, P., 2020. Paleogene carbonate systems of Saint Barthélemy, Lesser Antilles: stratigraphy and general organization. Newsletters on Stratigraphy, doi:10.1127/nos/2020/0587.

Cornée, J.-J., Léticée, J.-L., Münch, P., Quillévéré, F., Lebrun, J.-F., Moissette, P., Braga, J.C., Melinte-Dobrinescu, M., De Min, L., Oudet, J., Randrianasolo, A., 2012. Sedimentology, palaeoenvironments and biostratigraphy of the Pliocene-Pleistocene carbonate platform of Grande-Terre (Guadeloupe, Lesser Antilles forearc). Sedimentology 59, 1426-1451, doi:10.1111/j.1365-3091.2011.01311.x.

Cornée, J.-J., Munch, P., Philippon, M.M., BouDagher-Fadel, M., Quillévéré, F., Melinte-Dobrinescu, M., Leveneur, E., Gay, A., Meyer, S., Léticée, J.-L., Marcaillou, B., Laurencin, M., Klingelhoefer, F., Lebrun, J.-F., Lallemand, S., 2019. Oligocene to Pliocene paleogeography of the northern Lesser Antilles arc. AGU Fall Meeting San Francisco, 9-13 Dec, https://agu.confex.com/agu/fm19/meetingapp.cgi/Paper/509947.

De Min, L., Lebrun, J.-F., Cornée, J.-J., Münch, P., Léticée, J.-L., Quillévéré, F., Melinte-Dobrinescu, M., Randrianasolo, A., Marcaillou, B., Zami, F., 2015. Tectonic and sedimentary architecture of the Karukéra spur: A record of the Lesser Antilles fore-arc deformations since the Neogene. Marine Geology 363, 15-37, doi:10.1016/j.margeo.2015.02.007.

DeMets, C., Jansma, P.E., Mattioli, G.S., Dixon, T.H., Farina, F., Bilham, R.G., Calais, E., Mann, P., 2000. GPS geodetic constraints on Caribbean-North America plate motion. Geophysical Research Letters 27, 437-440, doi:10.1029/1999GL005436.

Deplus, C., 1998. Aguadomar cruise, RV L'Atalante, doi:10.17600/98010120.

Deville, E., Mascle, A., 2012. The Barbados ridge: A mature accretionary wedge in front of the Lesser Antilles active margin, in: Roberts, D.G., Bally, A.W. (Eds.), Principles of Geologic Analysis, pp. 581-607, doi:10.1016/B978-0-444-53042-4.00021-2.

Deville, E., Mascle, A., Callec, Y., Huyghe, P., Lallemant, S., Lerat, O., Mathieu, X., Padron de Carillo, C., Patriat, M., Pichot, T., Loubrieux, B., Granjeon, D., 2015. Tectonics and sedimentation interactions in the east Caribbean subduction zone: An overview from the Orinoco delta and the Barbados accretionary prism. Marine and Petroleum Geology 64, 76-103, doi:10.1016/j.marpetgeo.2014.12.015.

Embley, R.W., Langseth, M.G., 1977. Sedimentation processes on the continental rise of northeastern South America. Marine Geology 25, 279–297, doi:10.1016/0025-3227(77)90058-5.

Escalona, A., Mann, P., 2011. Tectonics, basin subsidence mechanisms, and paleogeography of the Caribbean-South American plate boundary zone. Marine and Petroleum Geology 28, 8-39, doi:10.1016/j.marpetgeo.2010.01.016.

Evain, M., Galvé, A., Charvis, P., Laigle, M., Kopp, H., Bécel, A., Weinzierl, W., Hirn, A., Flueh, E.R., Gallart, J., 2013. Structure of the Lesser Antilles subduction forearc and backstop from 3D seismic refraction tomography. Tectonophysics 603, 55-67, doi:10.1016/j.tecto.2011.09.021.

Feuillet, N., Beauducel, F., Tapponnier, P., 2011. Tectonic context of moderate to large historical earthquakes in the Lesser Antilles and mechanical coupling with volcanoes. J. geophys.Res. 116, doi:10.1029/2011JB008443.

Feuillet, N., Manighetti, I., Tapponnier, P., Jacques, E., 2002. Arc parallel extension and localization of volcanic complexes in Guadeloupe, Lesser Antilles. J. geophys.Res. 107, 2331, doi:10.1029/2001JB000308.

Grevemeyer, I., Ranero, C.R., Ivandic, M., 2018. Structure of oceanic crust and serpentinization at subduction trenches. Geosphere, doi:10.1130/ges01537.1.

Grindlay, N.R., Mann, P., Dolan, J.F., Van Gestel, J.-P., 2005. Neotectonics and subsidence of the Northern Puerto-Rico-Virgin Islands margin in response to the oblique subduction of high-standing ridges, in: Mann, P. (Ed.), Active tectonics and seismic hazards of Puerto Rico, the Virgin Islands and offshore areas. Geol. Soc. Am. Spec. Paper, pp. 31-60.

Heeszel, D.S., Wiens, D.A., Shore, P.J., Shiobara, H., Sugioka, H., 2008. Earthquake evidence for along-arc extension in the Mariana Islands. Geochem. Geophys Geosyst 9, n/a-n/a, doi:10.1029/2008gc002186.

Hensen, C., Wallmann, K., Schmidt, M., Ranero, C.R., Suess, E., 2004. Fluid expulsion related to mud extrusion off Costa Rica—A window to the subducting slab. Geology 32, 201, doi:10.1130/g20119.1.

Hirn, A., 2001. SISMANTILLES 1 cruise report, RV Nadir, , doi:10.17600/1080060.

Jany, I., Scanlon, M., Mauffret, A., 1990. Geological interpretation of combined Seabeam, Gloria and seismic data from Anegada Passage (Virgin Islands, north Caribbean). Marine Geophysical Research 12, 173-196, doi:10.1007/BF02266712.

Klingelhoefer, F., Marcaillou, B., Laurencin, M., Biari, Y., Laigle, M., Graindorge, D., Evain, M., Kopp, H., Lallemand, S., Lebrun, J.-F., Paulatto, M., 2018. Relation Between the Nature of the Subducting Plate, Heat Flow and Fluid Escape Structures at the Lesser Antilles Island arc. American Geophysical Union Fall Meeting Washington, D.C., 10-14 Dec 2018.

Laigle, M., Becel, A., de Voogd, B., Sachpazi, M., Bayrakci, G., Lebrun, J.-F., Evain, M., Group, t.T.W.R.S.R.w., 2013. Along-arc segmentation and interaction of subducting ridges with the Lesser Antilles Subduction forearc crust revealed by MCS imaging. Tectonophysics 603, 32-54, doi:10.1016/j.tecto.2013.05.028.

Laigle, M., Lebrun, J.-F., Hirn, A., 2007. SISMANTILLES 2 cruise report, RV L'Atalante,, doi:10.17600/7010020.

Laurencin, M., Graindorge, D., Klingelhoefer, F., Marcaillou, B., Evain, M., 2018. Influence of increasing convergence obliquity and shallow slab geometry onto tectonic deformation and seismogenic behavior along the Northern Lesser Antilles zone. Earth and Planetary Science Letters 492, 59-72, doi:10.1016/j.epsl.2018.03.048.

Laurencin, M., Marcaillou, B., Graindorge, D., Klingelhoefer, F., Lallemand, S.E., Laigle, M., Lebrun, J.-F., 2017. The polyphased tectonic evolution of the Anegada Passage in the northern Lesser Antilles subduction zone. Tectonics 36, doi:10.1002/2017TC004511.

Laurencin, M., Marcaillou, B., Graindorge, D., Lebrun, J.-F., Klingelhoefer, F., Boucard, M., Laigle, M., Lallemand, S., Schenini, L., 2019. The Bunce Fault and Strain Partitioning in the Northern Lesser Antilles. Geophysical Research Letters 46, doi:10.1029/2019GL083490.

Lebrun, J.-F., 2009. Kashallow 2 cruise, RV le Suroît. doi:10.17600/9020010.

Lebrun, J.-F., Lallemand, S.E., 2017. GARANTI Cruise, RV L'Atalante, doi:10.17600/17001200.

Legendre, L., Philippon, M., Münch, P., Léticée, J.-L., Noury, M., Maincent, G., Cornée, J.-J., Caravati, A., Lebrun, J.-F., Mazabraud, Y., 2018. Trench Bending Initiation: Upper Plate Strain Pattern and Volcanism. Insights From the Lesser Antilles Arc, St. Barthelemy Island, French West Indies. Tectonics 37, 2777-2797, doi:10.1029/2017TC004921.

Leroy, S., Mauffret, A., Patriat, P., Mercier de Lépinay, B., 2000. An alternative interpretation of the Cayman trough evolution from a reidentification of magnetic anomalies. Geophys. J. Int. 141, 539-557, doi:10.1046/j.1365-246x.2000.00059.x.

Léticée, J.-L., Cornée, J.-J., Münch, P., Fietzke, J., Philippon, M., Lebrun, J.-F., De Min, L., Randrianasolo, A., 2019. Decreasing uplift rates and Pleistocene marine terraces settlement in the central lesser Antilles fore-arc (La Désirade Island, 16°N). Quaternary International 508, 43-59, doi:10.1016/j.quaint.2018.10.030.

Lindsay, J.M., Robertson, R.E.A., Shepherd, J.B., Ali, S.T., 2005. Volcanic Hazard Atlas of the Lesser Antilless. Seismic Research Unit, The University of the West Indies, Trinidad and Tobago, W.I., p.

Lopez, A.M., Stein, S., Dixon, T.H., Sella, G., Calais, E., Jansma, P., Weber, J.C., Lafemina, P., 2006. Is there a northern Lesser Antilles forearc block? Geophysical Research Letters 33, L07317, doi:10.1029/2005GL025293.

Mann, P., Calais, E., Ruegg, J.P., DeMets, C., Jansma, P.E., Mattioli, G.S., 2002. Oblique collision in the northeastern Caribbean from GPS measurements and geological observations. Tectonics 6, 1057, doi:10.1029/2001TC001304.

Mann, P., Hippolyte, J.C., Grindlay, N.R., Abrams, L.J., 2005. Neotectonics of southern Puerto Rico and its offshore margin, in: Mann, P. (Ed.), Active tectonics an seismic hazards of Puerto Rico, the Virgin Inslands and off-shore areas. Geol. Soc. Am. Spec. Paper, pp. 115-138.

Mann, P., Taylor, F.W., Edwards, R.L., Ku, T., 1995. Actively evolving microplate formation by oblique collision and sideways motion along strike-slip faults:Anexample from the northeastern Caribbean plate margin. Tectonophysics 246, 1–69, doi:10.1016/0040-1951(94)00268-E.

Marcaillou, B., Klingelhoefer, F., 2013a. ANTITHESIS-1-Leg1 Cruise, RV L'Atalante, doi:10.17600/13010070.

Marcaillou, B., Klingelhoefer, F., 2013b. ANTITHESIS-1-Leg2 Cruise, RV Pourquoi Pas?, doi:10.17600/13030100.

Marcaillou, B., Klingelhoefer, F., 2016. ANTITHESIS-3 Cruise, RV Pourquoi Pas?, doi:10.17600/16001700.

Martin-Kaye, P.H.A., 1969. A summary of the geology of the Lesser Antilles, . Overseas Geology and Mineral Resources Bristish Geological Survey 10.

Mascle, J., Martin, L., 1990. Shallow structure and recent evolution of the Aegean Sea: A synthesis based on continuous reflection profiles. Marine Geology 94, 271-299, doi:10.1016/0025-3227(90)90060-W.

Masson, D.G., Scanlon, K.M., 1991. The neotectonic setting of Puerto Rico. GSA Bulletin 103, 144-154, doi:10.1130/0016-7606(1991)103<0144:TNSOPR>2.3.CO;2.

McCabe, R., 1984. Implications of paleomagnetic data on the collision-related bending of island arcs. Tectonics 4, 409–428, doi:10.1029/TC003i004p00409.

McCann, W.R., Sykes, L.R., 1984. Subduction of aseismic ridges beneath the Caribbean Plate: Implications for the tectonics and seismic potential of the northeastern Caribbean. J. geophys.Res. 89, 4493-4519, doi:10.1029/JB089iB06p04493.

Münch, P., Lebrun, J.-F., Cornée, J.-J., Thinon, I., Guennoc, P., Marcaillou, B., Bégot, J., Bertrand, G., Bes de Berc, S., Biscarrat, K., Claud, C., De Min, L., Fournier, F., Gailler, L., Graindorge, D., Léticée, J.-L., Marie, L., Mazabraud, Y., Melinte-Dobrinescu, M., Moissette, P., Quillévéré, F., Vérati, C., Randrianasolo, A., 2013. Pliocene to Pleistocene carbonate systems of the Guadeloupe archipelago, French Lesser Antilles: a land and sea study (the KaShallow project). Bulletin de la Société Géologique de France 184, 99-110, doi:10.2113/gssgfbull.184.1-2.99.

Nakamura, M., 2004. Crustal deformation in the central and southern Ryukyu Arc estimated from GPS data. Earth and Planetary Science Letters 217, 389-398, doi:10.1016/s0012-821x(03)00604-6.

Neill, I., Kerr, A.C., Hastie, A.R., Stanek, K.-P., Millar, I.L., 2011. Origin of the Aves Ridge and Dutch–Venezuelan Antilles: interaction of the Cretaceous 'Great Arc' and Caribbean–Colombian Oceanic Plateau? Journal of Geophysical Research B: Solid Earth 168, 333-347, doi:10.1144/0016-76492010-067.

Pelletier, B., Dupont, J., 1990. Effets de la subduction de la ride de Louisville sur l'arc des Tonga-Kermadec. Oceanologica Acta 10, 57-76.

Philippon, M., Cornée, J.-J., BouDagher-Fadel, M., Münch, P., Boschman, L.M., Van Hinsbergen, D.J.J., Gailler, L., Quillévéré, F., Léticée, J.-L., Lallemand, S., Lebrun, J.-F., 2019. Greater Antilles in the Lesser Antilles: lessons from Eocene thrusting at St. barthelemey island. AGU Fall meeting San Francisco, T31D-0271, 9-13 Dec. 2019, https://agu.confex.com/agu/fm19/meetingapp.cgi/Paper/537434.

Philippon, M., van Hinsbergen, D.J.J., Boschman, L.M., Gossink, L.A.W., Cornée, J.-J., BouDagher-Fadel, M., Léticée, J.-L., Lebrun, J.-F., Munch, P., 2020. Caribbean intra-plate deformation: Paleomagnetic evidence from St. Barthélemy Island for post-Oligocene rotation in the Lesser Antilles forearc. Tectonophysics 777, 228323, doi:10.1016/j.tecto.2020.228323.

Pichot, T., Patriat, M., Westbrook, G.K., Nalpas, T., Gutscher, M.-A., Roest, W.R., Deville, E., Moulin, M., Aslanian, D., Rabineau, M., 2012. The Cenozoic tectonostratigraphic evolution of the Barracuda Ridge and Tiburon Rise at the western end of the North America-South America plate boundary zone. Marine Geology 303-306, 154-171, doi:10.1016/j.margeo.2012.02.001.

Pindell, J.L., Barrett, S.F., 1990. Geological evolution of the Caribbean Region, in: Dengo, G., Case, J.E. (Eds.), The Caribbean Region. Geol. Soc. Am., Boulder, CO, pp. 405-433, doi:10.1130/DNAG-GNA-H.405.

Pindell, J.L., Kennan, L., 2009. Tectonic evolution of the Gulf of Mexico, Caribbean and northern South America in the mantle reference frame: an update. Geological Society, London, Special Publications 328, 1-55, doi:10.1144/SP328.1.

Reid, J.A., Plumley, P.W., Schellekens, J.H., 1991. Paleomagnetic evidence for late Miocene counterclockwise rotation of North Coast carbonate sequence, Puerto Rico. Geophysical Research Letters 18, 565-568, doi:10.1029/91GL00401.

Rodríguez-Zurrunero, A., Granja-Bruña, J.L., Carbó-Gorosabel, A., Muñoz-Martín, A., Gorosabel-Araus, J.M., Gómez de la Peña, L., Gómez Ballesteros, M., Pazos, A., Catalán, M., Espinosa, S., Druet, M., Llanes, P., ten Brink, U., 2019. Submarine morpho-structure and active processes along the North American-Caribbean plate boundary (Dominican Republic sector). Marine Geology 407, 121-147, doi:10.1016/j.margeo.2018.10.010.

Ryan, H.F., Scholl, D.W., 1989. The evolution of the forearc structures along an oblique convergent margin, central Aleutian arc. Tectonics 8, 497-516.

Schellart, W.P., 2010. Evolution of Subduction Zone Curvature and its Dependence on the Trench Velocity and the Slab to Upper Mantle Viscosity Ratio. J. geophys.Res. 115, doi:10.1029/2009jb006643.

ten Brink, U.S., Lin, J., 2004. Stress interaction between subduction earthquakes and forearc strike-slip faults: Modeling and application to the northern Caribbean plate boundary. J. geophys.Res. 109, B12310, doi:10.1029/2004JB003031.

Vannucchi, P., Galeotti, S., Clift, P.D., Ranero, C.R., von Huene, R., 2004. Long-term subduction erosion along the Middle America trench offshore Guatemala. Geology 32, 617-620, doi:10.1130/G20422.1.

Verschuur, D.J., Berkhout, A.J., Wapenaar, C.P.A., 1992. Adaptive surface-related multiple elimination Geophysics 57, 1166-1177, doi:10.1190/1.1443330.

Vogt, P.R., Lowrie, A., Bracey, D.R., Hey, R.N., 1976. Subduction of aseismic ocean ridges: Effects on shape, seismicity and other characteristics of consuming plate boundaries. Geological Society of America Special Paper, 172, p. 59.

von Huene, R., Lallemand, S.E., 1990. Tectonic erosion along the Japan and Peru convergent margins. GSA Bulletin 102, 704-720, doi:10.1130/0016-7606(1990)102<0704:TEATJA>2.3.CO;2.

von Huene, R., Ranero, C.R., Vannucchi, P., 2004. Generic model of subduction erosion. Geology 32, 913-916.

Wallace, L.M., Ellis, S., Mann, P., 2009. Collisional model for rapid fore-arc block rotations, arc curvature, and episodic back-arc rifting in subduction settings. Geochem. Geophys Geosyst 10, doi:10.1029/2008gc002220.

Westbrook, G.K., Mascle, A., Biju-Duval, B., 1984. Geophysics and the structure of the Lesser Antilles forearc, in: Biju-Duval, B., Moore, J.C. (Eds.), Initial Reports of the Deep Sea Drilling Project, pp. 23-38.

Wright, A., 1984. Sediment distribution and depositional processes operating in the Lesser Antilles intraoceanic island arc, eastern Caribbean, in: Biju-Duval, B., Moore, J.C. (Eds.), Initial Reports of the Deep SeaDrilling Project 78A-78B, pp. 301–324.

Figures and Tables

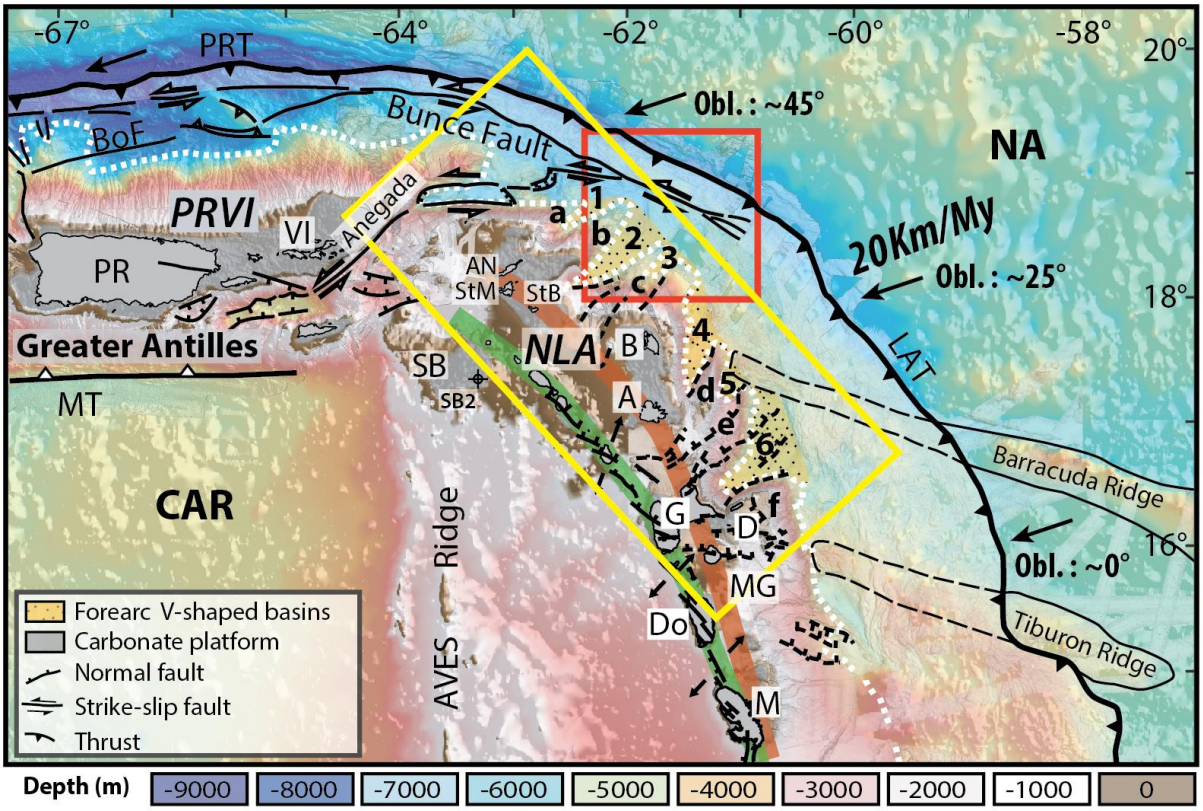

Figure 1: Regional bathymetric map of the Northern Lesser Antilles Subduction Zone (GEBCO 2014 dataset – WGS84 - UTM20). Plates: Caribbean (CAR), North American (NA). Margin segments: Puerto Rico Virgin Islands (PRVI), Northern Lesser Antilles (NLA). Trenches: Lesser Antilles Trench (LAT), Muertos Trough (MT), Porto Rico Trench (PRT). Islands and plateaus: Antigua (A), Anguilla (An), Barbuda (B), La Désirade (D), Dominica (Do), Guadeloupe (G), Martinique (M), Marie-Galante (MG), Saba Bank (SB), Saint Barthelemy (SB), Saint Martin (StM), Virgin Island (Vi). V-shaped valleys: Anguilla valley (1), Saint-Barthelemy valley (2), Barbuda valley (3), Antigua valley (4), Meduse Basin (5), La Désirade valley (6). Spurs: Maliana Spur (a), Tintamarre Spur (b), North and South Barbuda Spurs (c), Man of War Spur (d), Bertrand (South) and Falmouth (North) Spurs (e), Karukéra Spur (f); SB2: Petroleum drill Saba 2. Red line: remnant volcanic arc (mid Eocene - early Miocene). Green line: active arc (Pliocene to Present day). Black arrows: relative plates motion. Yellow and red frames: indicate location of Figure 2 and 3 respectively.

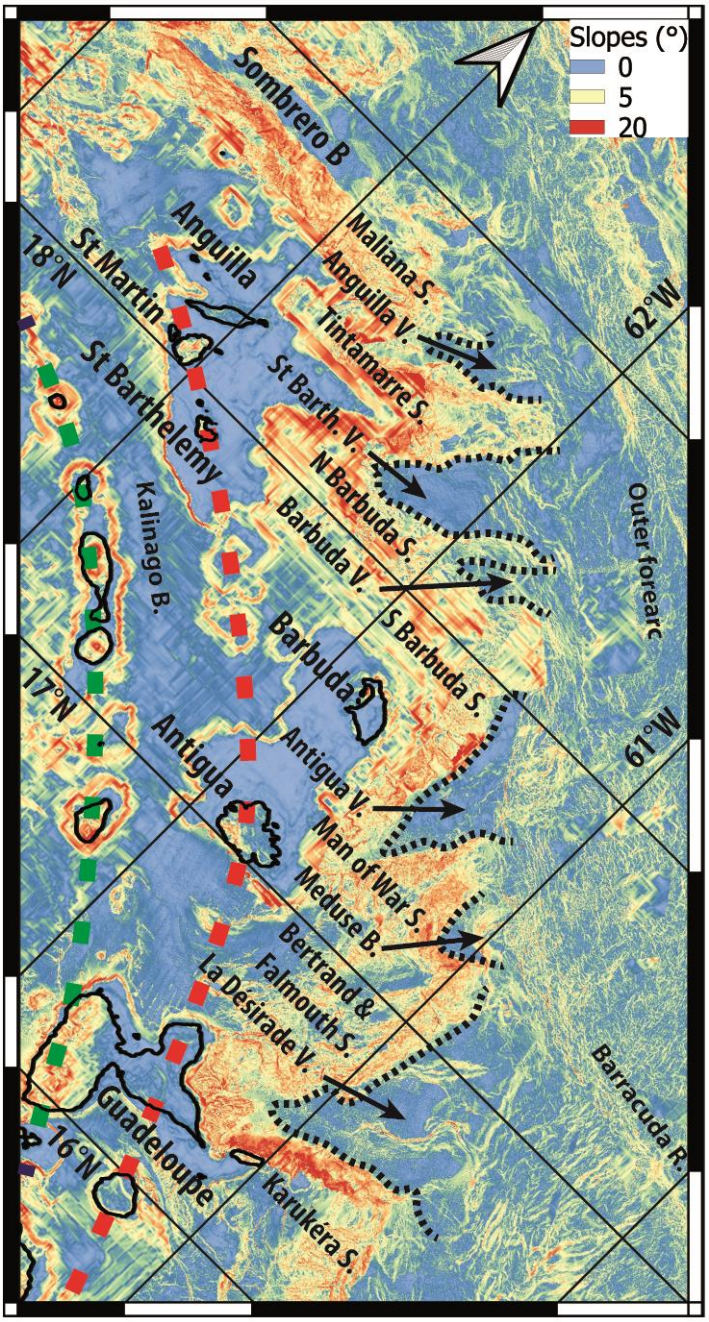

Figure 2: Relief slope map calculated from the GEBCO 2014 and ANTITHESIS data set. Abbreviations: V. for valley, S. for Spur, B. for basin, R. for ridge. See yellow frame in Figure 1 for location.

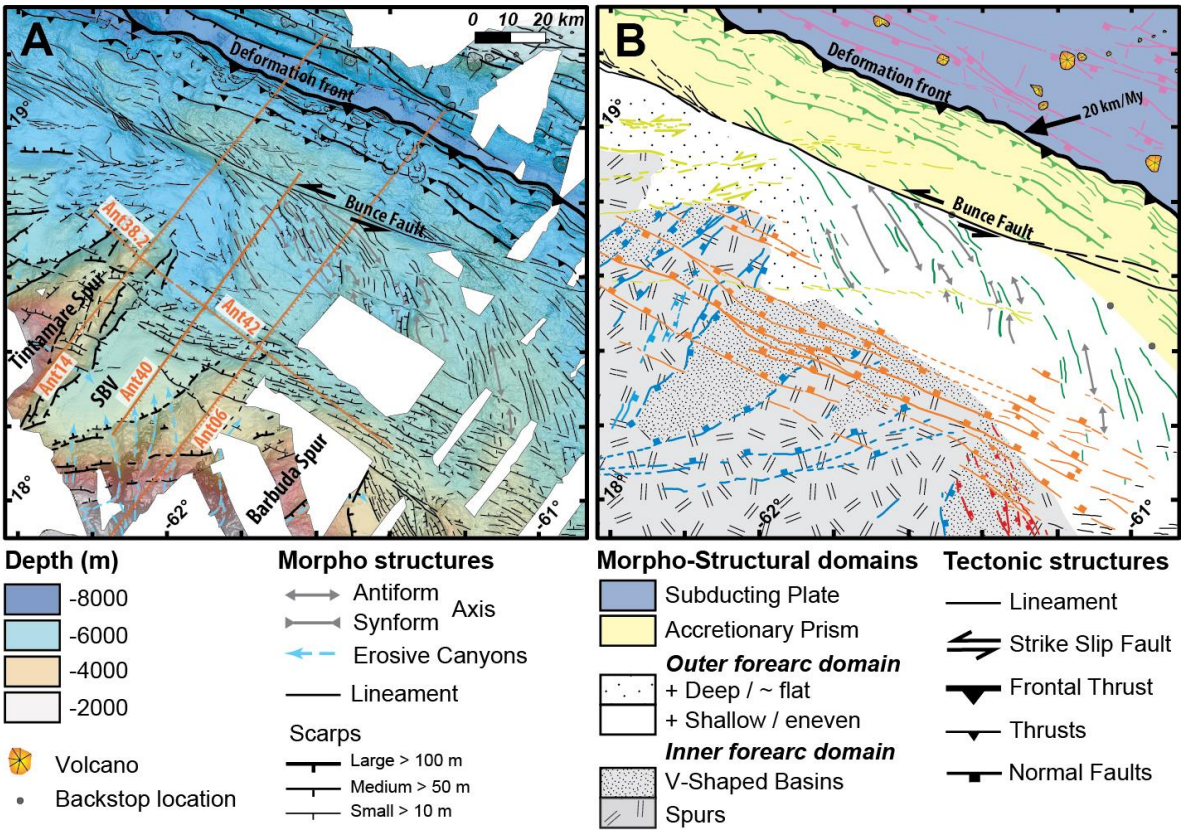

Figure 3: A) Detail bathymetric map with morphostructural interpretation for the St Barthelemy Valley (SBV), Tintamarre and south Barbuda Spurs at the Northern Lesser Antilles Margin. B) Tectonic map for the same area. From south to north, yellow, orange and red lines show N340°, N300° and N280°-trending faults. Blue lines show N-20-50°- and N60-90°-trending faults that bound the V-shaped basins. See red frame in Figure 1 for location.

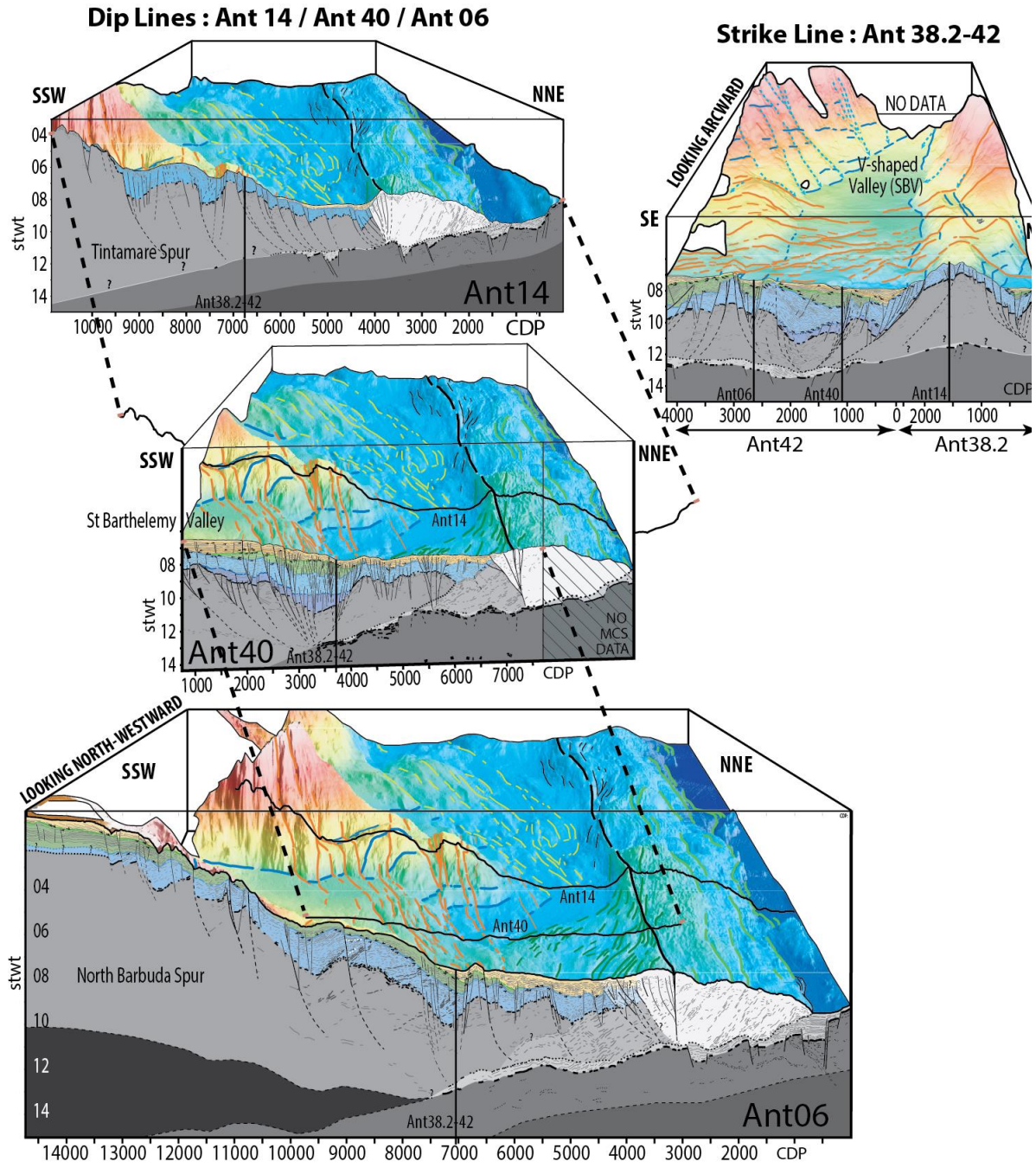

Figure 4: Three-dimensional seismic bathymetry view for lines Ant14, 40, 06, 38.2 and 42 (see solid orange lines in Figure 3 for location). Seismic line interpretation details and un-interpreted data are in supplementary material.

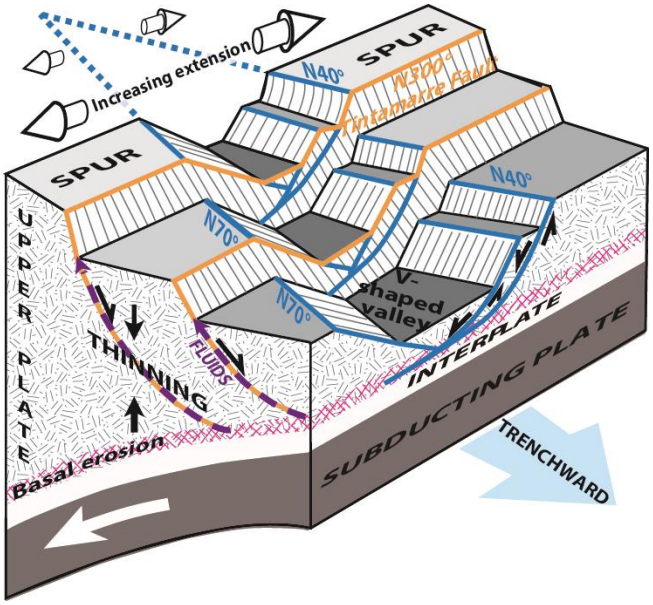

Figure 5: 3D conceptual model of V-shaped basin structures and the Tintamarre Faults Zone showing possible paths for fluids escape and hydration at the base of the upper plate enhancing subduction erosion processes at the Northern Lesser Antilles Forearc.

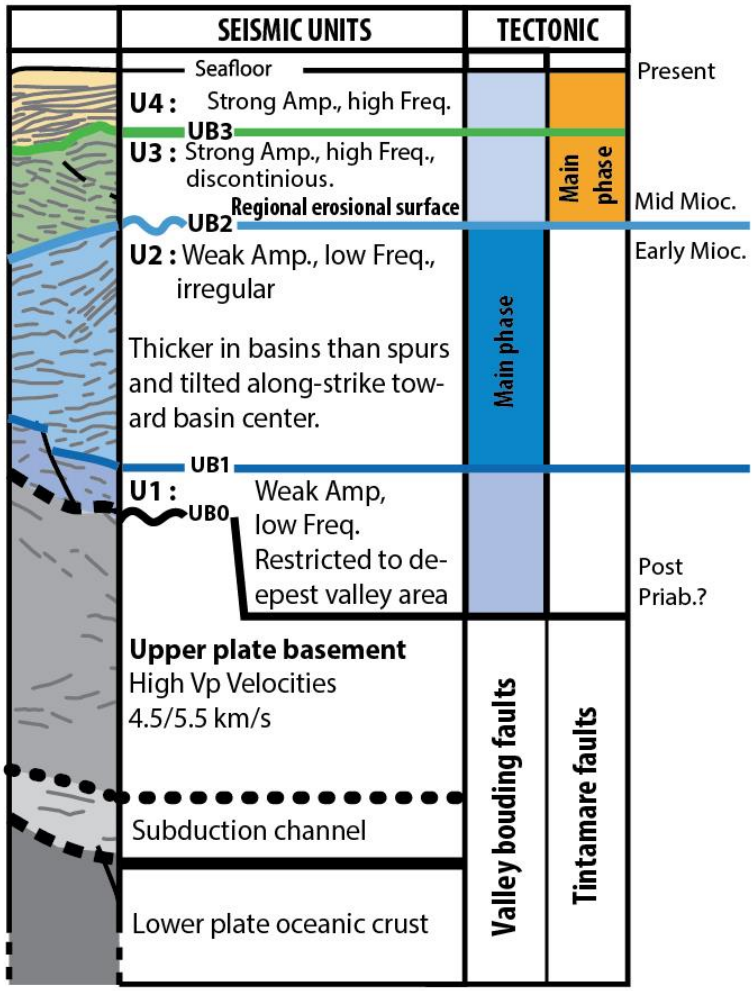

Figure 6: Stratigraphic log for the main unit facies and the main tectonic phases of fault systems at the St Barthelemy Valley and the Tintamarre and Barbuda Spurs.

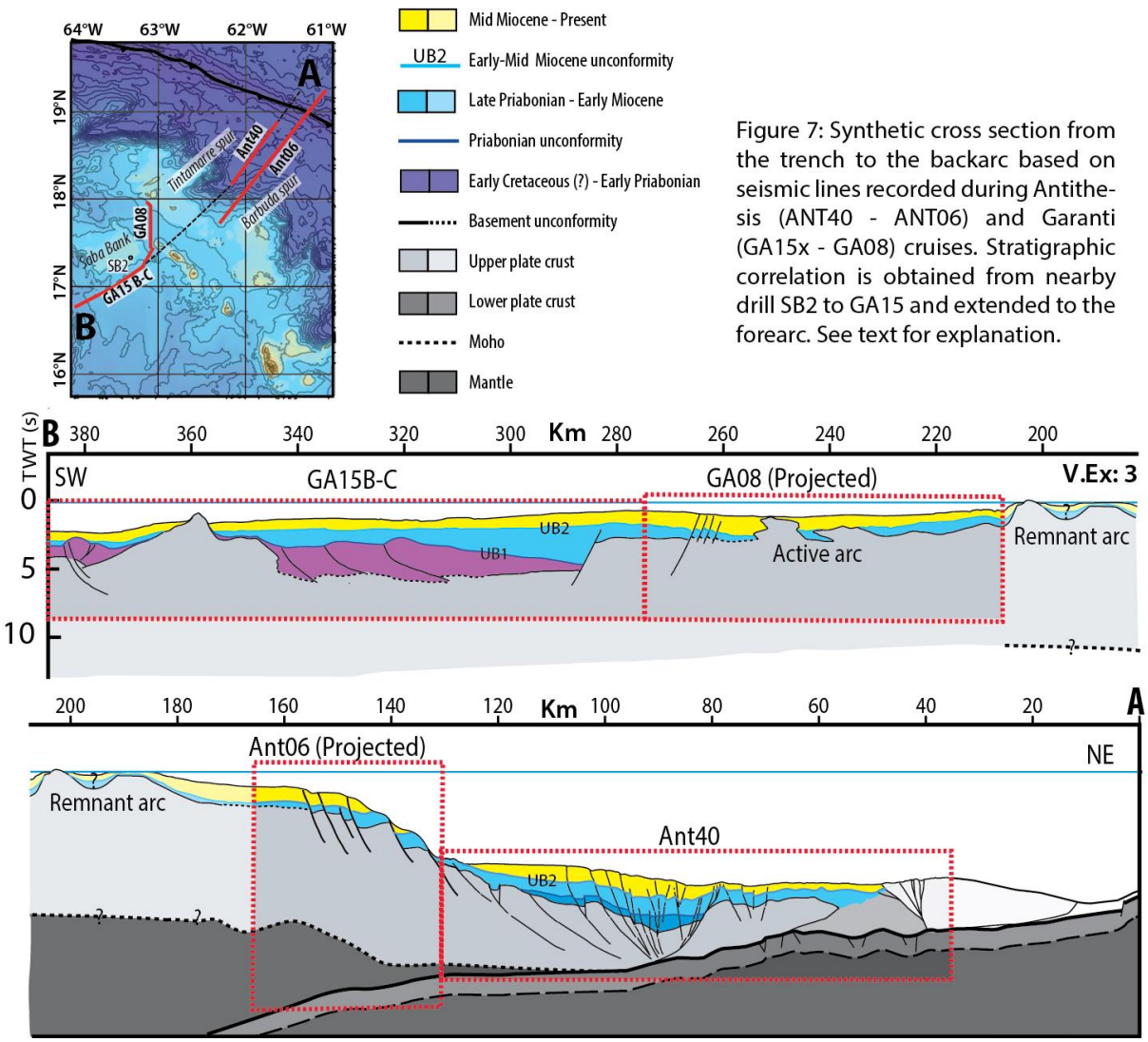

Figure 7: Synthetic cross section from the trench to the backarc based on seismic lines recorded during Antithesis (ANT40 - ANT06) and Garanti (GA15x - GA08) cruises. Stratigraphic correlation is obtained from nearby drill SB2 to GA15 and extended to the forearc. See text for explanation.

Figure 7

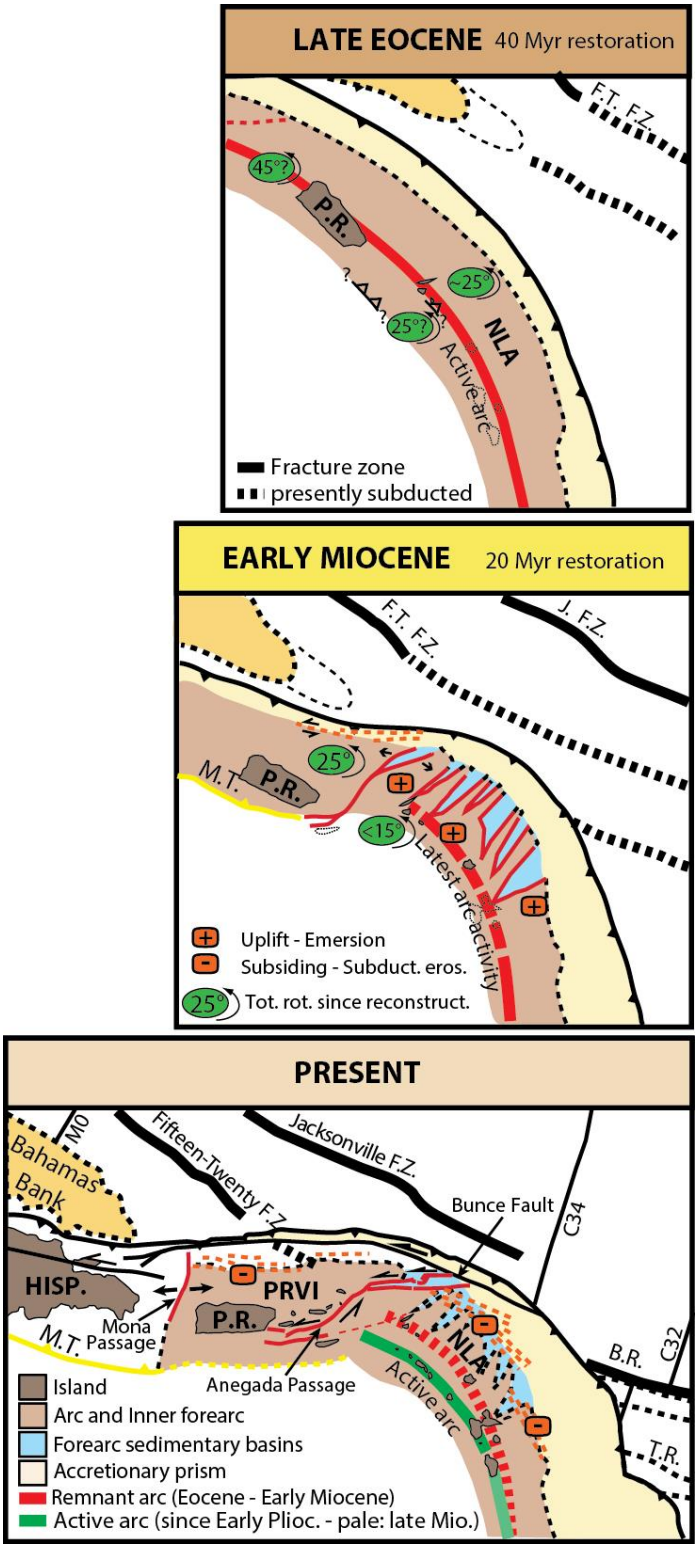

Figure 8: Kinematic reconstruction of the Northern Lesser Antilles Subduction Zone since 40Ma modified from Calais et al (2016). Caribbean Plate fixed. Guadeloupe Island (thin dots in all figures) is considered fixed with the Caribbean Plate interior. Puerto Rico (PR) is back rotated as indicated but its exact location is speculative and based on a geometric restoration across the Anegada Passage. BR: Barracuda Ridge, FT: Fifteen Twenty, FZ: Fracture Zone, Hisp: Hispaniola, J: Jacksonville; MT: Muertos Trough, TR: Tiburon Ridge.

Seismic Line	Ant06-DL	Ant14-DL	Ant38,2-SL	Ant40-DL	Ant42-SL
Survey	Antithesis I		Antithesis III		
Airgun array (in^3)	7699		6500		
Shot interval (s)	60		60		
Shot spacing (m)	154		150		
Shot number			189	605	523
Record time (s)	25		20		
Traces number	300	288	720		
Data sampling (ms)	2		2		
Traces spacing (m)	12.5		6.25		
Fold coverage	12		54	56	56
Acquisition speed (Kn)	5		5		

Table 1: Acquisition parameters of MCS during ANTITHESIS 1 and 3 cruises

Supplementary material

Annex 1: Along-dip seismic line ANT06 (time cross section) and interpretation. See Figure 3 for location.

Annex 2: Along-dip seismic line ANT40 (time cross section) and interpretation. See Figure 3 for location.

Annex 3: Along-dip seismic line ANT14 (time cross section) and interpretation. See Figure 3 for location.

Annex 4: Along-strike seismic line ANT38.2-42 (time cross section) and interpretation. See Figure 3 for location.